

The system parameters of the polars MR Ser and ST LMi

T. Shahbaz¹ and Janet H. Wood²

¹*University of Oxford, Department of Physics, Nuclear Physics Laboratory, Keble Road, Oxford, OX1 3RH, UK*

²*Keele University, Department of Physics, Keele, Staffordshire, ST5 5BG, UK*

30 August 2018

ABSTRACT

We obtain the Na I $\lambda 8183,8195$ absorption line radial velocity curves for the polars ST LMi and MR Ser, from which we find the semi-amplitudes to be $K_{abs}=329\pm 6$ km s⁻¹ and $K_{abs}=289\pm 9$ km s⁻¹ respectively. We find that for both systems the effects on the Na I absorption lines due to X-rays heating the inner face of the secondary are negligible, and so the values obtained for K_{abs} can be taken as the true semi-amplitude of the secondary star. We then determine the projected rotational velocities, $V_{rot} \sin i$, to be 104 ± 9 km s⁻¹ and 66 ± 13 km s⁻¹ for ST LMi and MR Ser respectively which enables their mass ratios to be calculated. For ST LMi and MR Ser we find the mass ratio to be 0.22 ± 0.04 and 0.10 ± 0.05 respectively; values which are significantly different only at the 94 percent level. Using the value for the orbital inclination derived from polarimetric measurements, we determine the mass, and the orbital and rotational velocities of the secondary stars. These are significantly different at less than the 90 percent level. However, if the limb darkening is the same in both objects, these quantities are significantly different at the 96 percent level.

We present Doppler maps of the Na I absorption and Ca II emission in ST LMi and MR Ser. In both systems the Na I absorption covers the secondary star. In ST LMi the Doppler image of the Ca II emission shows that it originates at the inner face of the secondary star. In MR Ser, however, the emission lies close to but not on the secondary star.

We show that “spike” in the orbital period distribution of polars is a significant feature, although the discovery of only one more system with a period outside the “spike” would decrease its significance below a 99 percent confidence level. We conclude that, even if the limb darkening coefficients for the secondary stars in ST LMi and MR Ser are the same, we cannot rule out the two systems having identical parameters. Therefore our observations are compatible with the theory explaining the “spike” in the period distribution of the AM Hers.

Key words: binaries: – close – stars: fundamental parameters – stars: individual: ST LMi – stars: individual: MR Ser – cataclysmic variables

1 INTRODUCTION

AM Her type systems consist of a magnetic white dwarf primary star accreting material from a late type M dwarf secondary star. The white dwarf primary star has a strong enough magnetic field ($B > 10$ MG) to lock it into synchronous rotation with the orbit. If one compares the orbital period distribution of the AM Hers with that of the non-magnetic CVs, then one finds that the main features of the CV distribution re-appear in the form of a minimum period $P_{orb}=78$ m, and the period “gap” between $P_{orb}=2-3$ hrs (Wheatley 1995). However, there are three obvious features in the AM Her period distribution (1) a concentration of systems near $P_{orb}=114$ m (the “spike”), no such feature

occurs in the distribution of weakly magnetic CVs; (2) a long period cut-off, significantly shorter than that for CVs, and (3) more systems in the period “gap” than for CVs.

Cataclysmic variables evolve from longer to shorter periods, ceasing mass transfer as they pass through the period “gap”. The period “gap” has been modelled in terms of an interruption of orbital angular momentum loss at 3 hrs, allowing the secondary star to relax into thermal equilibrium and detach from its Roche lobe. Systems regain contact at 2 hrs after orbital angular momentum loss through gravitational radiation. The “spike” in the polar distribution has been explained as being the period at which most polars come out of the period “gap” (Hameury, King & Lasota 1990). However, it has been shown that for the “spike” to

be so narrow, for those systems in the “spike”, the masses of the secondary stars must ALL be $0.200 \pm 0.002 M_{\odot}$ AND the masses of the white dwarfs must only differ by $\sim 0.05 M_{\odot}$ (Ritter & Kolb 1992). Therefore not only do we expect the mass ratios for the systems in the “spike” to be approximately the same, but the general system parameters such as the orbital velocities should also be almost identical. To test this theory the system parameters of polars and in particular those in the spike must be determined more accurately than before. This can be done by measuring the radial velocity of the secondary star, K_2 , and its rotational velocity, $V_{rot} \sin i$. In the red region of the spectrum, where the M dwarf is expected to contribute significantly to the observed flux, the spectra of polars are usually dominated by cyclotron radiation, which originates in the post-shock flow near the magnetic pole of the white dwarf, thus making observations of the red component difficult. However, when they enter the low state and the accretion ceases, or in parts of the orbit where the accreting region is occulted it becomes much easier to observe the secondary star (see Cropper 1990 for a review).

In this paper we report on the use of medium resolution, phase resolved spectroscopy to study the orbital motion of the secondary stars in ST LMi, MR Ser, AM Her and 1H 1752+081. We measure $V_{rot} \sin i$ and K_2 for MR Ser and ST LMi and deduce their system parameters. We also measure $V_{rot} \sin i$ for AM Her and attempt to do so for 1H 1752+081. The polars MR Ser, ST LMi and 1H 1752+081 lie in the “spike”. We also discuss the likelihood of the “spike” being a genuine feature and if our observations of ST LMi and MR Ser are compatible with theoretical explanations of the “spike”.

2 OBSERVATIONS AND DATA REDUCTION

MR Ser, ST LMi, AM Her and 1H 1752+081 were observed with the ISIS spectrograph attached to the 4.2-m William Herschel Telescope on the nights of 1994 March 24/25 and 25/26. Here we only present the results from the red arm. The EEV CCD was used with the R600R grating giving a dispersion of $0.74 \text{ \AA pixel}^{-1}$. On the first night the wavelength coverage was 7800–8586Å but on the second night the central position was moved to give 8030–8888Å coverage. Our principal aim was to determine radial velocities and to measure the rotational broadening of the absorption line, so we used a narrow slit (1.0 arcsec) which resulted in a spectral resolution of $1.9\text{\AA} \text{ (FWHM)} \equiv 70 \text{ km s}^{-1}$. Further observational details are contained in Table 1. The seeing on the first night was steady at about 1 arcsec, and on the second night it was typically between 0.5 and 1.2 arcsecs. The spectral type of the secondary star in AM Her has been determined by many authors to be M5 (see Southwell et al. 1995 and references within). Mukai & Charles (1987) determined the spectral type of the secondary stars in ST LMi and MR Ser to be M5.5. We therefore also observed Gl 406 (M6V) and Gl 473 (M5V) which we use for cross-correlation in the next section. We took care to observe this star through the slit of the same width as used for the two targets. The flux standard Feige 34 (Oke & Gunn 1983) was observed using wide and narrow slits on each night to correct for the instrumental response. Cu-Ar arc exposures were taken ev-

ery 30-40 min in order to calibrate the wavelength scale. We binned the CCD pixels on readout into groups of three pixels along the slit. The effect of this was to reduce the readout noise and deadtime of the CCD.

Sensitivity variations were removed with a balance frame prepared from tungsten-lamp flat-fields. Third order polynomial fits to the sky were subtracted, and raw spectra were then extracted using the optimal algorithm of Horne (1986), which weights the pixels along the spatial direction in order to obtain the maximum signal-to-noise ratio. The arc spectra were extracted with the same weights and at the same position as the target, and fitted with third-order polynomials. The rms scatter of the fits was $\sim 1/20$ th of a pixel. With four coefficients fitted to about 20 lines in each case, the statistical uncertainty in the wavelength scale is therefore of the order $1/45$ th of a pixel. This corresponds to an uncertainty of 0.6 km s^{-1} .

Atmospheric features were removed from the red arm spectra by using a wavelength calibrated water template star produced from the observed standard star. The template star was then corrected to the zenith distance (z) of the object by multiplying by a factor of $(\sec z)^{0.6}$. A comparison of the tabulated absolute flux values with a spline fit to the continuum of the flux standard provided a correction for the large-scale instrumental response.

3 RESULTS

3.1 Radial velocities of ST LMi and MR Ser

We obtained absorption line radial velocity curves using the Na I $\lambda 8183, 8194$ doublet and also emission line radial velocity curves using the Ca II $\lambda 8498, 8542$ lines. K_{abs} and K_{emi} are defined as the semi-amplitude of the absorption and emission line radial velocity curves respectively. The heliocentric radial velocities of MR Ser and ST LMi are shown in Figures 1 and 2.

In order to measure the absorption line radial velocity curves we cross-correlated the individual spectra with the template star spectrum (Tonry & Davis 1979), only using the wavelength range close to the Na I absorption lines. Prior to cross-correlation, the spectra were interpolated onto a logarithmic wavelength scale. Three spectra from ST LMi and eighteen from MR Ser were too noisy to obtain a reliable cross-correlation peak, and were not used for the fit. Gl 406 (M6V) was used as the template spectrum. We find K_{abs} to be $329 \pm 6 \text{ km s}^{-1}$ and $289 \pm 9 \text{ km s}^{-1}$ for ST LMi and MR Ser, respectively.

For each of MR Ser and ST LMi, to obtain the template spectrum for the Ca II triplet emission lines we obtained a preliminary template by averaging the spectra using K_{abs} . The summed spectrum showed some double peaked structure implying that the velocity used to correct for the Doppler motion was incorrect, and was not the velocity of the regions producing the Ca II emission. We then performed the cross correlation to obtain K_{emi} , only using the wavelength range which contained the Ca II $\lambda 8498, 8542$ emission lines. This value was then used to Doppler correct the original spectra to give the final template spectrum for the Ca II emission, in which the emission was narrow and single peaked. We find K_{emi} to be $213 \pm 4 \text{ km s}^{-1}$ and $173 \pm 1 \text{ km s}^{-1}$ for ST LMi and MR Ser, respectively.

Because cataclysmic variables have very short periods, it is generally believed that any initial non-circularity would have been quickly removed by tidal forces between the red star and the white dwarf, and that the present orbits are indeed circular. However, Davey and Smith (1992) argue that the radial velocity curves may still be distorted from a pure sine wave by geometrical distortion and heating of the secondary star by its companion, causing the centre of light given by the strength of the Na I doublet to differ from the centre of mass. The effects of this can be represented by allowing for a phase shift in the sine curve, or more generally by introducing a fictitious eccentricity. They describe a procedure for detecting any effects of heating on the radial velocity curve. Firstly one must check for the significance of a fit with an eccentric orbit. If the fit is not significantly better than a purely sinusoidal fit, then the semi-amplitude of the curve K_{abs} measured from the absorption features represents a measure of the true semi-amplitude of the radial velocity curve of the secondary star K_2 .

For both systems we found that the fit to the absorption line radial velocity curve with an eccentric orbit was not significantly better than that with a circular orbit. We obtained eccentricities of 0.027 ± 0.017 and 0.075 ± 0.046 for ST LMi and MR Ser, for which the significance of the eccentricity parameter was less than 50 percent. Therefore the measured value of K_{abs} from the absorption lines can be taken to represent the true value of K_2 . After adding the heliocentric radial velocity of the template star (13 km s^{-1} ; Gliese 1969) we determined K_2 using a circular fit of the form

$$V(\phi) = \gamma + K_2 \sin(2\pi\phi) \quad (1)$$

to the absorption and emission line heliocentric radial velocities (see Table 2). Here γ is the systemic velocity and ϕ is the phase angle of the observations with $\phi=0.0$ at inferior conjunction (i.e. when the red dwarf is in front of the white dwarf). The ephemerides derived for ST LMi and MR Ser (see Table 2) agree well with those of Mukai & Charles (1987). Figures 3 and 4 show the Doppler corrected average spectra of the two targets.

As another check to see if there is any effect due to heating, we fitted the Na I radial velocities measured only between phases -0.2 and $+0.2$, when the secondary star is viewed from the back and its appearance should be relatively unaffected by the effects of irradiation. We find that the value for K_{abs} does not change within the uncertainties. Our derived values for K_2 from the sinusoidal fit to the radial velocity curve are comparable with those derived by Mukai & Charles (1987). However there seems to be some discrepancy in the value for γ , which may be explained by the fact that there are some inconsistencies between the published radial velocity for most red dwarfs (Friend et al. 1990). In order to check our γ velocity estimates we performed the cross correlation analysis using a fake template star, having the instrumental resolution of the data, and the main absorption and emission lines present at their rest wavelengths. This implies that the fake template star has no γ velocity associated with it. We found that our derived parameters agreed well with those obtained earlier. Despite this, it should be noted for the emission line case, that using the Doppler averaged sum of the target star as a template star for the emission line data may in some way bias the de-

termination of the emission line γ velocity. The result may depend on the phase chosen as the reference phase for the average spectrum. Therefore, the only reliable estimate of the γ velocity from the emission lines is that obtained using the fake template star.

3.2 AM Her and 1H 1752+081

Our data were less extensive for AM Her and 1H 1752+081. For AM Her we cross-correlated the template star Gl 473 (M5V) with the target spectra in order to determine the velocity shift. We then Doppler corrected and summed the spectra. The mean spectrum is shown in Figure 5. For 1H 1752+081 the signal-to-noise ratio of the data was such that we were unable to Doppler correct the spectra to the Na I radial velocity. We therefore merely show the summed spectrum in Figure 6. Only low resolution blue spectra exist for this source (Ferrario et al. 1995). Many emission lines can be seen in both objects such as He II $\lambda 8246$, Ca II $\lambda 8498$, 8542 , 8662 and the Paschen lines $\lambda 8598$, 8750 . In AM Her the Na I absorption lines are strong whereas they are weak in 1H 1752+081. Na I has not been observed in 1H 1752+081 previously.

3.3 The rotational broadening and mass ratio

In order to determine the rotational broadening, $V_{rot} \sin i$, we followed the procedure described by Marsh, Robinson and Wood (1994). We Doppler corrected and summed the spectra for our individual targets using K_{abs} . We then fitted the excess light from the system i.e. that not arising from the secondary star, plus a constant times a rotationally broadened version of the template star, to the object's spectrum. The template star was broadened by convolution with the rotational profile of Gray (1976) assuming a linearized limb darkening coefficient of $u = 0.72$, taken from Al-Naimiy (1978). The broadened templates and the excess light are shown for the individual objects in Figures 3, 4 and 5. A high pass filter was then applied to the difference spectrum to remove any large-scale spectral differences and then the χ^2 was computed. Fitting a parabola to the distribution of χ^2 versus broadening values, we obtain a minimum χ^2 for each target and so the best value for the rotational broadening.

For ST LMi and MR Ser we obtained $V_{rot} \sin i = 105 \pm 7$ and $66 \pm 12 \text{ km s}^{-1}$ respectively, and for AM Her we obtained $V_{rot} \sin i = 70 \pm 11 \text{ km s}^{-1}$. The latter is consistent with that obtained by Southwell et al. (1995). We were not able to determine $V_{rot} \sin i$ in 1H 1752+081. The $1-\sigma$ uncertainties in $V_{rot} \sin i$ were derived by forcing the minimum χ^2 to increase by 1 (Lampton, Margon & Bowyer 1976).

The analysis above gives the uncertainties assuming the limb darkening is known. However, in reality this is not the case. We therefore repeated the above procedure using no and full limb darkening. For $u = 0.0$ we find $V_{rot} \sin i = 98 \pm 7$, 60 ± 12 and $65 \pm 10 \text{ km s}^{-1}$ for ST LMi, MR Ser and AM Her respectively. For $u = 1.0$ we find $V_{rot} \sin i = 110 \pm 7$, 71 ± 12 and $72 \pm 12 \text{ km s}^{-1}$ for ST LMi, MR Ser and AM Her respectively. We therefore adopt $V_{rot} \sin i = 104 \pm 9 \text{ km s}^{-1}$ and $V_{rot} \sin i = 66 \pm 13 \text{ km s}^{-1}$ for ST LMi and MR Ser (see Figures 3 and 4). For AM Her we find $V_{rot} \sin i = 68 \pm 12 \text{ km s}^{-1}$ (see Figure 5).

Armed with K_2 and $V_{rot} \sin i$ we can now determine the mass ratio $q (= M_2/M_1)$. Assuming that the companion is tidally locked, spherically symmetric and fills its Roche lobe, the rotational broadening provides a measurement of the binary mass ratio through the result (see e.g. Wade & Horne 1988)

$$V_{rot} \sin i = 0.462 K_2 q^{1/3} (1 + q)^{2/3}. \quad (2)$$

Substituting our values for $V_{rot} \sin i$ and K_2 in equation (2) we find the mass ratios of ST LMi and MR Ser to be 0.22 ± 0.04 and 0.10 ± 0.05 respectively. (Since our results for AM Her are consistent with those of Southwell et al. (1995) and they have already determined the system parameters we do not do so here). The correction of $V_{rot} \sin i$ and q due to the Roche geometry only introduces an error of a few percent (Marsh et al 1994; Southwell et al 1995). We performed a t -test of the values obtained for the mass ratio for ST LMi and MR Ser and find that the values for the mass ratios are only significantly different at the 94 percent level (1.9σ).

However, if we assume that the two systems have the same limb darkening coefficient, for example $u = 0.72$, we then find the uncertainties in q for ST LMi and MR Ser are reduced to 0.03 and 0.05 respectively. Using these uncertainties, we then find that the mass ratios are significantly different at the 96 percent level. We thus conclude that even if we assume that the systems have similar limb darkening we cannot show at the 99 percent confidence level that the two systems have different mass ratios.

3.4 Doppler images

The emission lines from cataclysmic variables are broadened by Doppler shifting from the accretion disc (in weakly magnetic systems), component stars and mass transfer. Marsh & Horne (1988) have shown that it is possible to derive the distribution of emission from observations of the profile covering the binary orbit. Here we use the same technique but the features we are interested in are narrow and arise from the companion star or the accretion stream. The images are presented in velocity space rather than position coordinates, since there is no unique transform between velocity and position in accreting binaries.

Figures 7 and 8 show the Doppler maps of the Na I absorption and Ca II emission distribution for ST LMi and MR Ser respectively. We also place on the maps the path of the gas stream and the shape of the secondary star's Roche-lobe for the given values of K_2 and q . The Na I maps for both systems show absorption covering most of the secondary star, and the Ca II emission arising from regions near the inner Lagrangian point (L_1). It should be noted that the resolution of the Doppler maps is limited by the velocity dispersion of the data (see section 2).

The emission-line region is displaced towards the centre of mass of the binary system, making the observed velocity amplitude smaller than the true secondary star velocity. This “ K_2 ” correction (Wade & Horne 1988) can be expressed as

$$K_2 = \frac{K_{emi}}{1 - f(1 + q)(R_2/a)} \quad (3)$$

where R_2 is the distance from the L_1 point to the centre of

the secondary star, and $0 < f < 1$ expresses the distribution of line emission over the surface of the secondary star. Placing the emission entirely at the L_1 point i.e. $f=1$, for ST LMi using $K_{emi}=213 \pm 4 \text{ km s}^{-1}$ we find $K_2=313 \pm 13 \text{ km s}^{-1}$. This agrees with the value for K_2 obtained from the absorption lines. For MR Ser, the “ K_2 ” correction gives a value for K_2 much smaller than that obtained from the absorption line radial velocity curve. One requires $q > 0.35$ in order to obtain the observed K_2 . These results are consistent with the fact that the emission in the Doppler maps in ST LMi lies on the secondary star near L_1 , while in MR Ser it is close to L_1 but not on the secondary star.

The accretion stream can be divided into two distinct parts. The first part is free-falling in the orbital plane and the second is where the stream grabs onto the magnetic field lines at the magnetospheric radius. The phasing of the first narrow emission component would be offset from that of the absorption lines arising from the secondary star. The magnetic field in all AM Her type systems in which it has been measured has been found to be similar, including ST LMi (Schmidt, Stockman & Grandi 1983) and MR Ser (Wickramasinghe et al. 1991). For systems with periods less than 2 hrs like ST LMi and MR Ser the magnetospheric radius is very likely to be close to the L_1 point. Observations of ST LMi show that the white dwarf magnetospheric radius is $0.79\text{--}0.93 R_{L1}$ and in MR Ser R_{mag} is expected to be very similar (Mukai 1988; where R_{L1} is the distance of the inner Lagrangian point from the white dwarf). In MR Ser the emission we observe in velocity space is very close to the L_1 point. It could arise from an extended emission region around the L_1 point. If it is due to emission from the region where the free-falling gas stream joins onto the magnetic field lines of the white dwarf, then one would expect it to lie on the gas stream in the Doppler map. This is not the case.

4 DISCUSSION

4.1 The mass of the binary components

Given our values of K_2 and q combined with the orbital period, P , and the binary inclination, i , we can also determine the masses of the compact object and its companion using

$$\frac{K_2^3 P}{2\pi G} = \frac{M_1 \sin^3 i}{(1 + q)^2}. \quad (4)$$

The binary inclination for MR Ser and ST LMi can be obtained from polarimetric observations. For ST LMi and MR Ser we use inclination angles of $56^\circ \pm 4^\circ$ (Cropper 1988) and $45^\circ \pm 5^\circ$ (Brainerd & Lamb 1985) respectively. We find that the masses for the secondary stars in ST LMi and MR Ser are $M_2=0.17 \pm 0.07 M_\odot$ and $M_2=0.07 \pm 0.08 M_\odot$ respectively (see Table 2). Using the values for the inclination we can derive the orbital velocity, $V_{orb} = K_2/\sin i$, and the rotational velocity, V_{rot} , of the secondary star. For ST LMi and MR Ser we find V_{orb} to be $397 \pm 20 \text{ km s}^{-1}$ and $409 \pm 38 \text{ km s}^{-1}$, and V_{rot} to be $125 \pm 12 \text{ km s}^{-1}$ and $93 \pm 20 \text{ km s}^{-1}$ respectively. If we assume that the two systems have similar limb darkening, then the uncertainty in the V_{rot} measurements reduces to 10 km s^{-1} and 19 km s^{-1} for ST LMi and MR Ser respectively. Similarly, for V_{orb} the uncertainties become 20 and 38 km s^{-1} and for M_2 0.06 and $0.08 M_\odot$. The parameters

are still not significantly different at the 90 percent confidence level.

4.2 The “spike”

The sample of known AM Hers has more than doubled over the last 5 years, largely as a result of the ROSAT extreme ultraviolet and soft X-ray surveys. To date there is a total of 43 systems (see Table 3). In Table 4 we list some details of how the AM Hers are distributed. We set the lower and upper edges of the period “gap” to lie at 126 and 192 mins respectively. The upper edge of the whole distribution is taken to be at 300 mins. The outlier RXJ0515+01 with an orbital period of 479 mins is excluded from the analysis that follows because of its unusual nature. Its low magnetic field strength is somewhat of a surprise, because for a given white dwarf mass one would expect that the field strength required to enforce synchronism should increase significantly as the orbital period increases (Buckley & Shafter 1995).

There are two questions we want to answer in order to explain the observed characteristics of the period distribution (see Figure 9).

- What is the probability of the observed number of systems lying in the period “gap”?
- What is the probability of the “spike” occurring by a statistical fluke?

There are 42 AM Her systems in the period range used (see above), of which 4 are in the period “gap” which lies between 126 and 192 mins. Following the calculation of King 1994 (private communication) if the AM Hers are distributed uniformly in the range 78–300 mins, the probability of finding at least 4 systems in the period “gap” is given by

$$P(4 \text{ in “gap”}) = {}^N C_4 p^4 (1-p)^{N-4} \quad (5)$$

where ${}^N C_4$ is the number of ways of choosing 4 objects from a set of N , N is the total number of systems in the period range and p is the probability of an AM Her avoiding the “gap”. Using $N=42$, we find $p=(1-66/222)=0.703$, which implies $P(4 \text{ in “gap”})=1.3 \times 10^{-3}$, *i.e.* the observed number of systems in the gap is inconsistent with the distribution being uniform at the 99.9 percent level.

The pre-ROSAT data contained 12 members below the period “gap”, of which 6 were in a 2 min interval (the “spike”). In the current sample the number of “spike” members has risen to 9 at the cost of the “spike” broadening to 3 min. Suppose that there are M AM Her systems below the period gap, uniformly distributed over the period range of R mins, so that the probability of any one system being in a given interval of 3 mins is $3/R$. We want to know what is the probability of the remainder $M-1$ being distributed in such a way that $r-1$ of them (a total of r) will lie in the same 3 min interval, for any initial choice of interval. One has to add these results for each of the initial choices, which means multiplying by M . Thus

$$P(\text{“spike”}) = M {}^{M-1} C_{r-1} p^{r-1} (1-p)^{M-r}. \quad (6)$$

With $R=38$ mins corresponding to a range 78–116 mins (the most conservative), $M=25$ and $r=9$ systems in the “spike”, we find $P(\text{“spike”})=0.0068$, *i.e.* the probability that

the spike is genuine is 99.3 percent. Using the range 78–126 mins, $M=27$ and $r=9$ systems in the spike we find $P(\text{“spike”})=0.0030$ with a probability of 99.7 percent that it is genuine. The old (pre ROSAT launch) sample had 12 systems with 6 in a 1.2 min interval. Using data before the ROSAT detections, we find the probability of the “spike” occurring randomly was 0.00014.

Although the significance of the “spike” has reduced since the ROSAT mission, the “spike” is still a significant feature of the period distribution of the AM Hers. However, it would take only one new system in the period range 78–116 mins but outside the “spike” to raise the probability that a 9 member “spike” could be a random event to more than 1 percent.

It should be noted that equation (6) is the probability that any “spike” with an interval of 3 mins occurs below the “gap”. The question we should next ask, is what is the probability of the “spike” with r members occurring in a particular 3-min interval at 113–116 mins. This is given by

$$P(\text{“spike” at 113 – 116 mins}) = M C_r p^r (1-p)^{M-r} \quad (7)$$

Using $R=38$ mins (the most conservative), $M=25$ and $r=9$ systems in the “spike”, we find $P(\text{“spike” at 113–116 mins})=0.00007$, *i.e.* 99.99 percent. Thus the “spike” in the period distribution occurring at 113–116 mins is a significant feature.

If we compare the secondary star masses derived earlier for ST LMi and MR Ser, with that predicted by the “spike” theory of $0.200 \pm 0.002 M_\odot$ (Ritter and Kolb 1992), we find that we cannot show with certainty, *i.e.* at the 99 percent level, that the two systems have masses different from this theoretical mass. If we accept the spike theory, then the two systems should have almost identical system parameters, including q , M_2 , V_{orb} and V_{rot} . The values we have obtained for all the system parameters for ST LMi and MR Ser are such that we cannot rule out that the two systems have the same parameters. Even if the limb darkening coefficients are the same q can only be shown to be different at the 96 percent level. Our results are therefore compatible with the theoretical explanation of the spike given by Ritter and Kolb (1992). Given a value for the limb darkening the dominant source of uncertainty in the deduced system parameters, other than q , is the orbital inclination, i . To improve the sensitivity of this test of the spike theory a more accurate determination of i is required. Very high resolution spectroscopy is needed to reduce the error in $V_{rot} \sin i$. More systems in the spike should also be investigated.

5 CONCLUSIONS

We have obtained data of medium spectral and high time resolution covering the orbital cycles of the polars ST LMi and MR Ser. Our spectra allow us to determine the dwarf star’s radial velocity semi-amplitude, K_{abs} , using the Na I $\lambda 8183,8195$ absorption features. We find that for both systems the effects of irradiation on the Na I lines are negligible, since there is no distortion of the radial velocity curves from a pure sine wave. Therefore K_{abs} can be taken as the true semi-amplitude of the secondary star K_2 . We find that for ST LMi $K_{abs} = 329 \pm 6 \text{ km s}^{-1}$ and for MR Ser $K_{abs} = 289 \pm 9 \text{ km s}^{-1}$. Doppler maps of the

Na I distribution for the two systems are very similar, covering most of the secondary star. However, in contrast, the Ca II maps are somewhat different. In ST LMi, the map shows the emission arising from the secondary star at the inner Lagrangian point, probably due to heating of the inner face of the secondary star, whereas in MR Ser the emission is observed to arise from regions close to but not on the secondary star. For ST LMi if we assume all the emission arises from the L_1 point, then the semi-amplitude of the emission line radial velocity curve gives a value for K_2 consistent with that obtained from the absorption line radial velocity study.

The spectra of the secondary stars are significantly broadened by rotation. We determine this projected rotational broadening which enables us to determine the mass ratios of the systems. For ST LMi and MR Ser we find $q=0.22\pm 0.04$ and 0.10 ± 0.05 , respectively. Using the values for the inclination derived from polarimetric measurements, we find $M_2=0.17\pm 0.07 M_\odot$, $V_{orb} = 397 \pm 20 \text{ km s}^{-1}$ and $V_{rot} = 125 \pm 12 \text{ km s}^{-1}$ for ST LMi. For MR Ser we find $M_2=0.07\pm 0.08 M_\odot$, $V_{orb} = 409 \pm 38 \text{ km s}^{-1}$ and $V_{rot} = 93 \pm 20 \text{ km s}^{-1}$. We conclude that we cannot rule out the two systems having the same system parameters, therefore our observations are consistent with the theoretical explanation of the spike.

Finally we show that at present the ‘‘spike’’ is a significant feature of the period distribution of the AM Hers. However, the discovery of only one more system with a period that does not lie in the ‘‘spike’’ would decrease the significance of the spike below a 99 percent confidence level.

6 ACKNOWLEDGEMENTS

We are very grateful to our support astronomer Vik Dhillon for help above and beyond the call of duty. We thank Tom Marsh for the use of his PAMELLA, MOLLY and DOPPLER routines, and for his valuable support and suggestions. We also thank Tom Marsh and Karen Southwell for useful discussions. We thank the referee R.C. Smith for useful comments. TS was supported by a PPARC postdoctoral fellowship, and JHW by a PPARC Advanced fellowship. The WHT is operated on the island of La Palma by the Royal Greenwich Observatory in the Spanish Observatorio del Roque de los Muchachos of the Instituto de Astrofísica de Canarias. The data reduction was carried out on the Oxford Starlink node. Some of the figures were prepared using the ARK software.

REFERENCES

- Al-Naimiy H.M., 1978, *Ap&SS*, 53, 181
 Brainerd J.J., Lamb D.Q., 1985, *Proc. of the 7th North American Workshop on Cataclysmic Variables and Low Mass X-ray Binaries*, p. 247, eds Lamb D.Q., & Patterson J., Reidel, Dordrecht, Holland.
 Beuermann K., Thomas H.C., 1993, *Adv. Space Res.*, 13(12), 115
 Buckley D.A.H., Shafter A.W., 1995, *MNRAS*, 275, L61
 Cropper M.S., 1988, *MNRAS*, 231, 597
 Cropper M.S., 1990, *Space Sci. Rev.*, 54, 195
 Davey S.C., Smith R.C., 1992, *MNRAS*, 257, 476
 Ferrario L., Wickramasinghe D., Bailey J., Buckley D., 1995, *MNRAS*, 273, 17
 Friend M.T., Martin J.S., Smith R.S., Jones D.H.P., 1990, *MNRAS*, 246, 637
 Gliese W., 1969, *Veröff. Rechen-Inst. Heid.* No 22
 Gray D.F., 1976, *The Observations and Analysis of Stellar Photospheres*, Wiley-Interscience, New York
 Hameury J.M., King A.R., Lasota J.P., 1990, *MNRAS*, 242, 141
 Horne K., 1986, *PASP*, 98, 609
 Lampton M., Margon B., Bowyer S., 1976, *ApJ*, 208, 177
 Kolb U., de Kool M., 1994, *A&A*, 279, L5
 Marsh T.R., Horne K., 1988, *MNRAS*, 235, 269
 Marsh T.R., Robinson E.L., Wood J.H., 1994, *MNRAS*, 266, 137
 Mukai K., Charles P.A., 1987, *MNRAS*, 226, 209
 Mukai K., 1988, *MNRAS*, 232, 175
 Oke J.B., Gunn J.E., 1983, *ApJ*, 266, 713
 Reinsch, K., Burwitz V., Beuermann K., Schwöpe A.D., Thomas H. 1994, *A&A*, 291, 27
 Ritter H., Kolb U., 1992, *A&A*, 259, 159
 Ritter H., Kolb U., 1995, in *X-ray Binaries*, eds Lewin W., van Paradijs J., Van den Heuvel E., Cambridge University Press.
 Schmidt G D., Stockman H.S., Grandi S.A., 1983, *AApJ*, 271, 735
 Schwöpe A.D., Thomas, H., Beuermann K., 1993, *A&A*, 271, 25
 Southwell K.A., Still M.D., Smith R.C., Martin J.S., 1995, *A&A*, 302, 90
 Tonry J., Davis M., 1979, *AJ*, 84, 1511
 Wade R.A., Horne K., 1988, *ApJ*, 324, 411
 Wheatley P.J., 1995, *MNRAS*, 274, L51
 Wickramasinghe D.T., Cropper M., Mason K.O., Garlick M., 1991, *MNRAS*, 250, 692

Heliocentric radial velocity (kms^{-1})

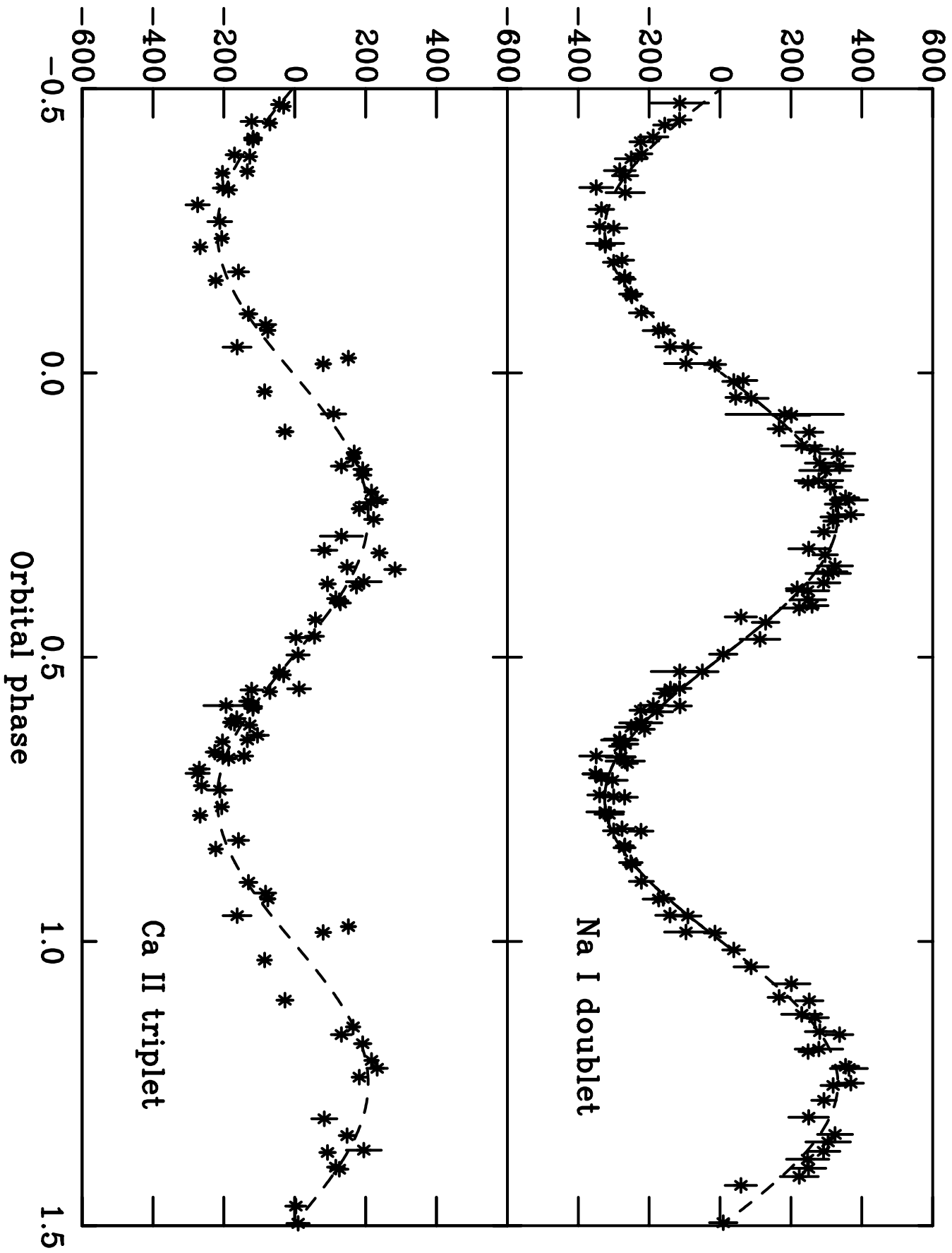


Table 1: Journal of observations

	ST LMi	MR Ser	AM Her	1H 1752+081
Night of observation	2	1,2	2	2
Number of spectra	88	80	4	4
Exposure time	170s \equiv 0.025 ϕ	170s \equiv 0.025 ϕ	280s \equiv 0.025 ϕ	170s \equiv 0.025 ϕ

Table 2: Derived parameters for ST LMi and MR Ser, Uncertainties are 1- σ assuming unknown limb darkening

Parameter	ST LMi	MR Ser
Period (days)	0.0791 \pm 0.0003	0.0789 \pm 0.0001
T ₀ (HJD - 2440000)	9438.5546 \pm 0.0003	9437.696 \pm 0.001
γ_{abs} (km s ⁻¹)	3 \pm 4	-50 \pm 7
γ_{emi} (km s ⁻¹)	-5 \pm 3	-51 \pm 2
K ₂ ^{abs} (km s ⁻¹)	329 \pm 6	289 \pm 9
K ₂ ^{emi} (km s ⁻¹)	213 \pm 4	173 \pm 1
V _{rot} sin i (km s ⁻¹)	104 \pm 9	66 \pm 13
Fraction of light from secondary	0.76 \pm 0.02	0.20 \pm 0.01
q	0.22 \pm 0.05	0.10 \pm 0.07
f(M ₁ /M _⊙)	0.29 \pm 0.02	0.20 \pm 0.02

Using the value for the inclination
derived from polarimetric measurements

i (°)	56 \pm 4	45 \pm 5
M ₁ (M _⊙)	0.76 \pm 0.30	0.67 \pm 0.70
M ₂ (M _⊙)	0.17 \pm 0.07	0.07 \pm 0.08
R ₂ (R _⊙)	0.20 \pm 0.04	0.15 \pm 0.08
a (R _⊙)	0.75 \pm 0.15	0.70 \pm 0.36
V _{orb} (km s ⁻¹)	397 \pm 20	409 \pm 38
V _{rot} (km s ⁻¹)	125 \pm 12	93 \pm 20

Heliocentric radial velocity (kms^{-1})

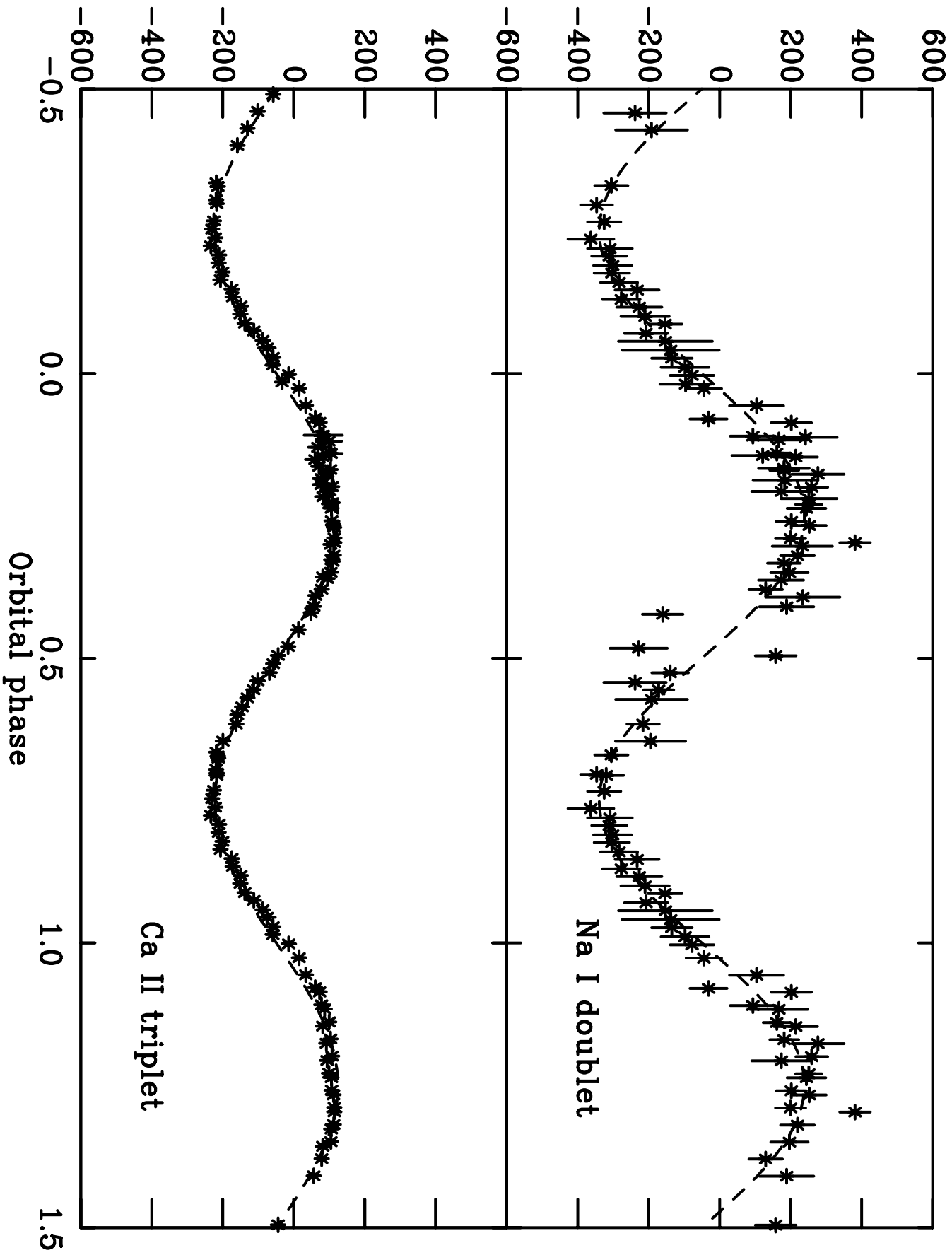


Table 4: AM Her period distribution parameters

Number of systems below the period “gap”	27
Number of systems above the period “gap”	11
Number of systems in the “spike”	9
Number of systems in the period “gap”	4
Total number of systems	42
Period range for “spike” (mins)	113-116
Period range for “gap” (mins)	126-192
Period range for whole distribution (mins)	78-300

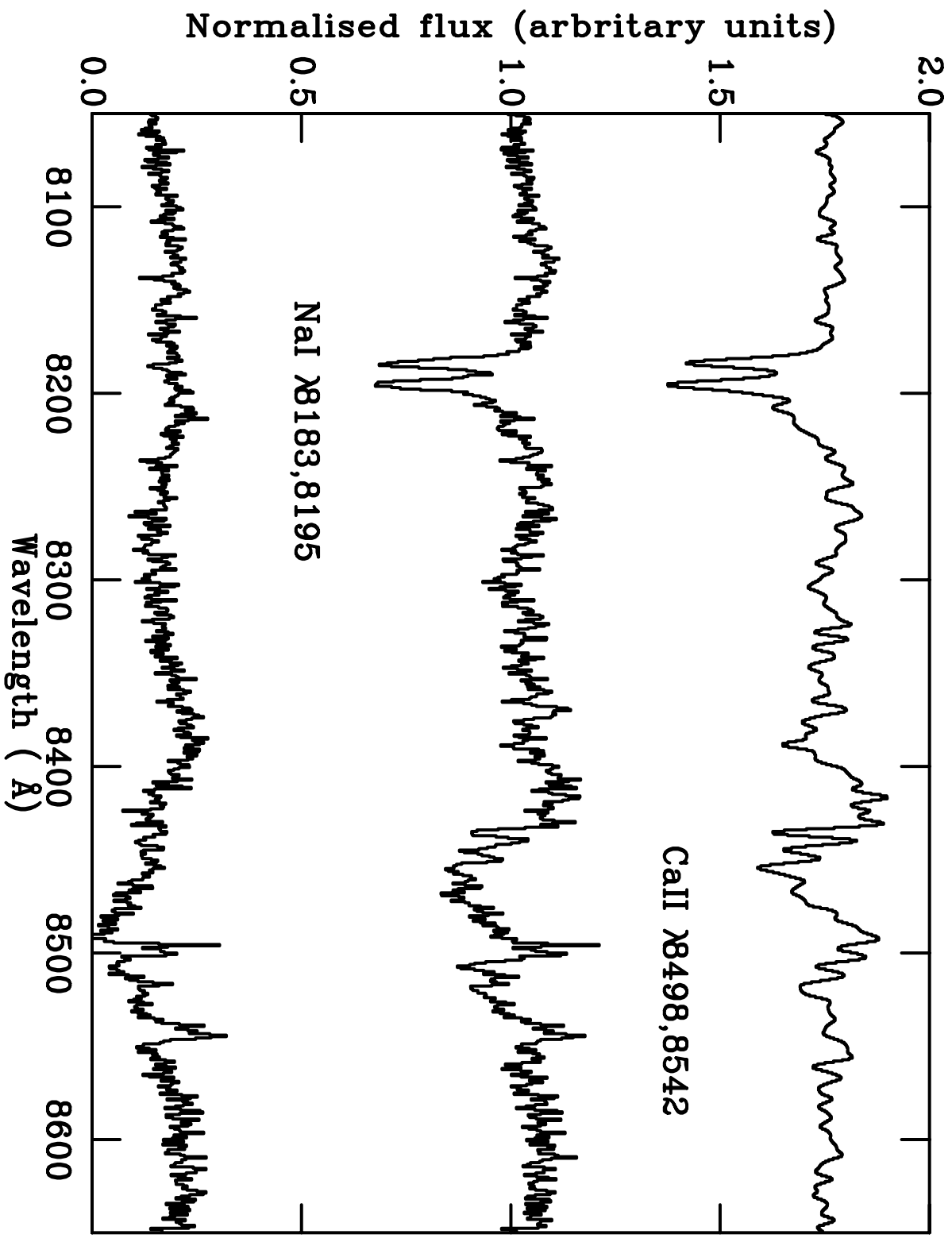
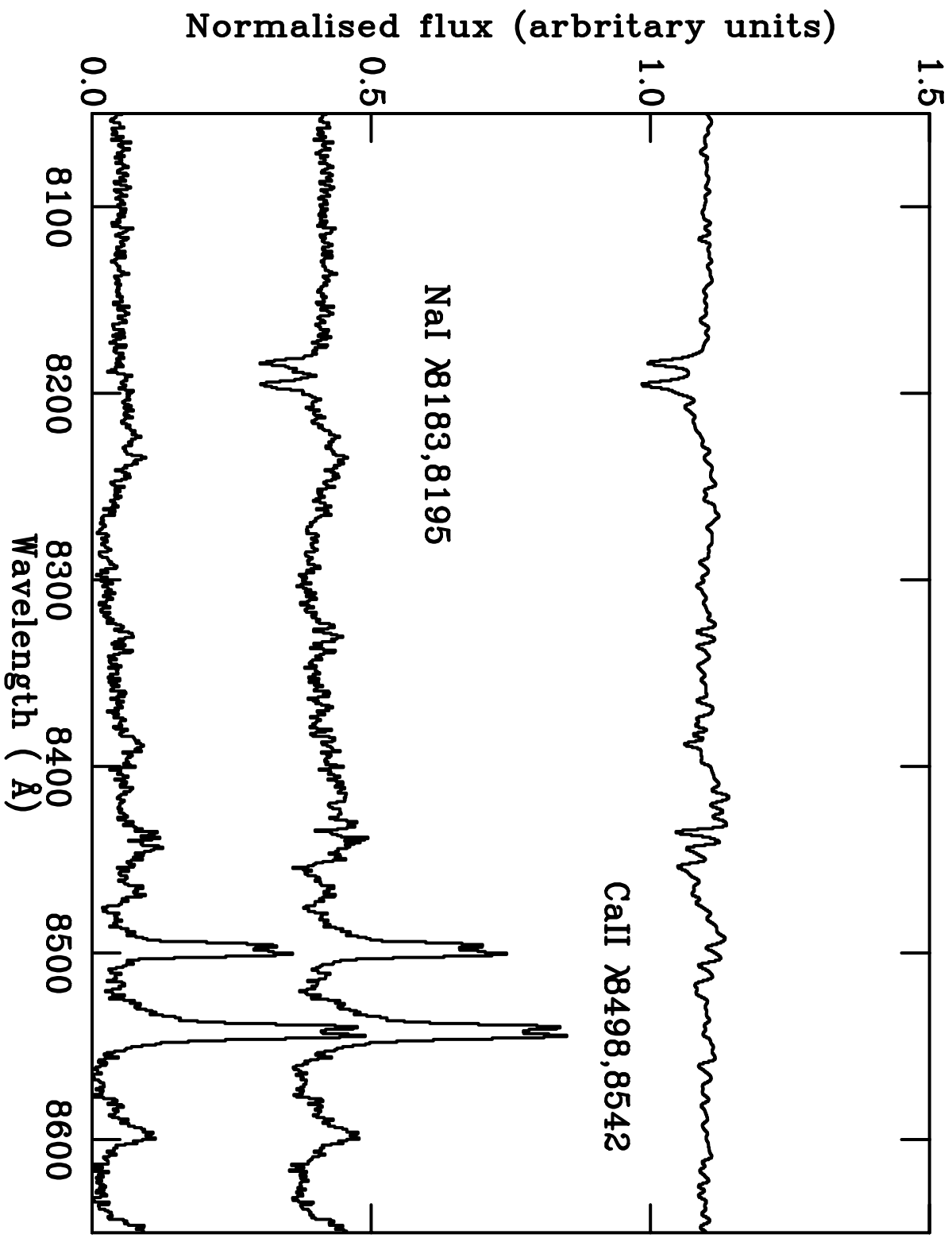
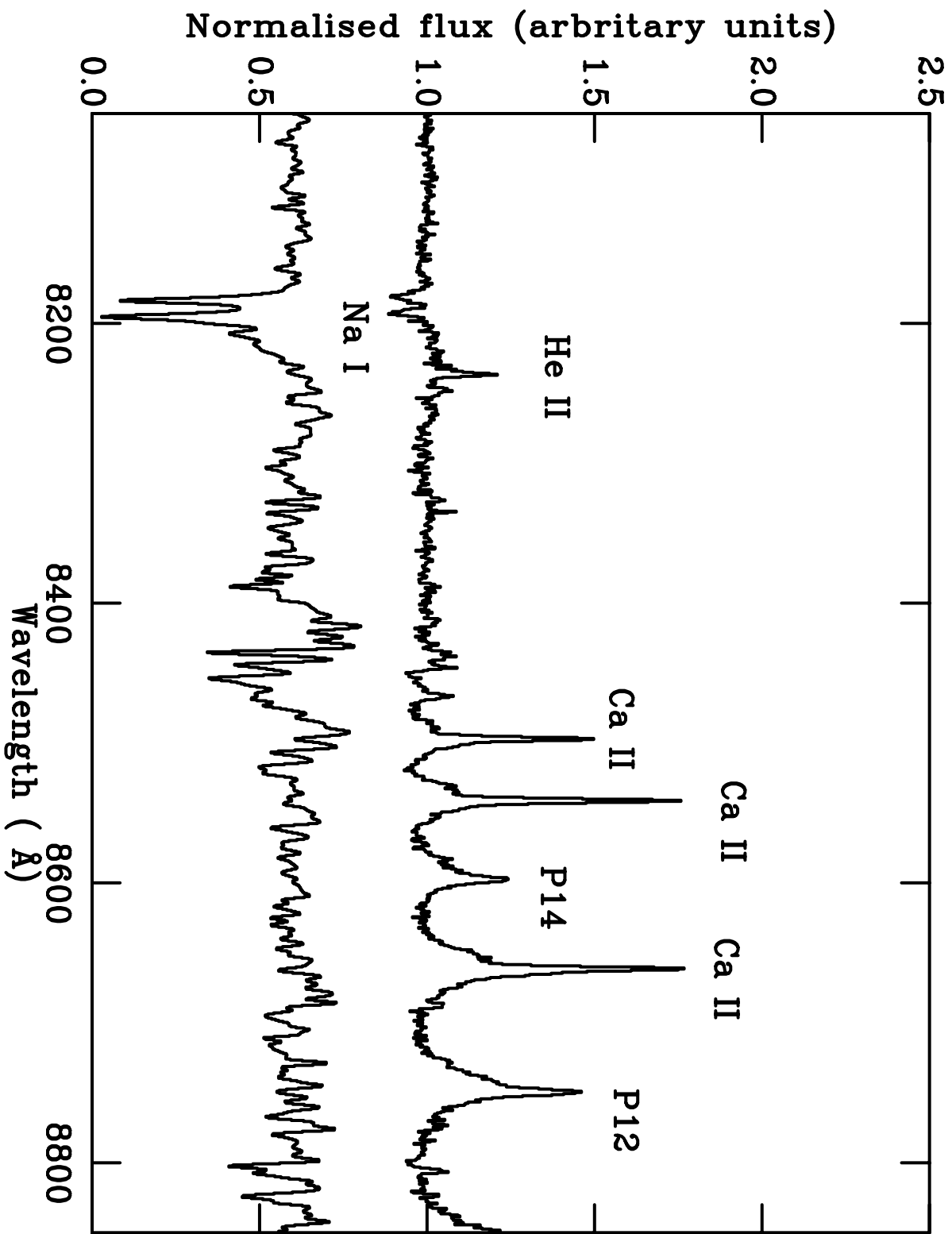


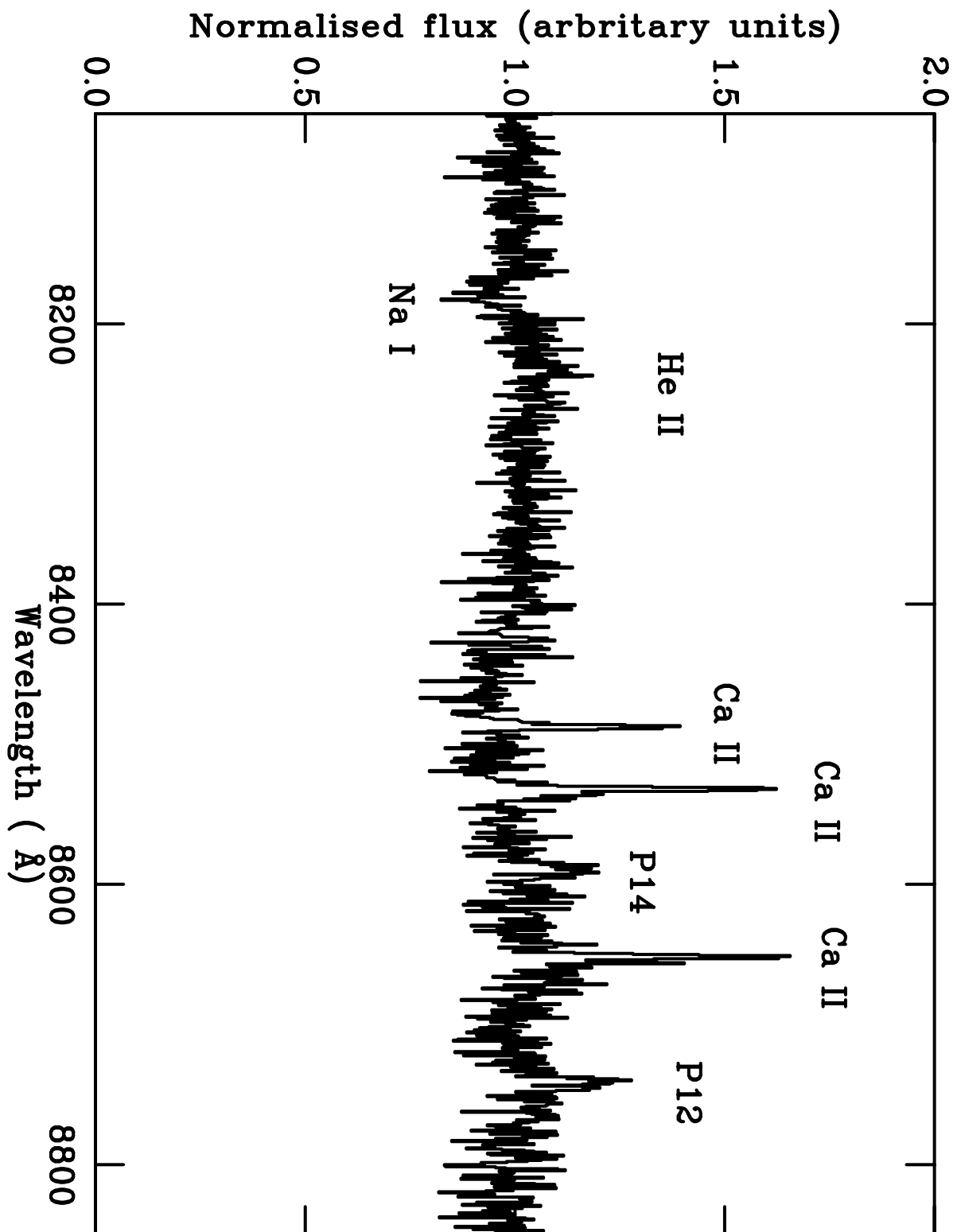
Table 3: Currently known AM Her systems in order of increasing orbital period

Name	P_{orb} (min)	i (degrees)
RX0132-65	78.0	
RE1307+535	79.7	
RX1015+09	80.0	
EF Eri	81.0	58 ± 12
RX0153-59	89.0	
DP Leo	89.8	76 ± 10
RE1149+28	90.0	
RE1844-74	90.0	
RX1957-57	99.0	
VV Pup	100.4	76 ± 6
V834 Cam	101.5	45 ± 9
RE0453-42	102.0	
EP Dra	104.6	~ 80
RE0501-03	107.0	
RX1002-19	107.0	
CE Cru	108.6	
1H 1752+081	113.0	$75-90$
RE1802+18	113.0	< 80
BL Hyi	113.6	70 ± 10
MR Ser	113.6	45 ± 5
ST LMi	113.9	56 ± 4
EK UMa	114.5	56 ± 19
WW Hor	114.6	
AM UMa	114.8	65 ± 5
1113+432	115.9	
RE2107-05	125.0	80 ± 5
EU Cnc	125.4	
UZ For	126.5	150 ± 12
RE0531-46	133.0	
RE1938-46	140.0	
Drissen V211B	160.0	
BY Cam	199.3	
AM Her	185.6	30 ± 5
V1500 Cyg	201.0	
RE1940-10	202.2	
RX0929-2404	203.4	
RX1007-20	208.0	
RX2316-05	209.0	
QQ Vul	222.5	60 ± 14
EXO 0329-26	228.4	
RX1313-32	252.0	
RX0203+29	275.5	
RE0515+01	479.0	

For systems discovered before the ROSAT mission, the data has been taken from Cropper (1990). For the post ROSAT systems, data has been taken from Ritter & Kolb (1995), Beuermann & Thomas (1993), Kolb & de Kool (1994).



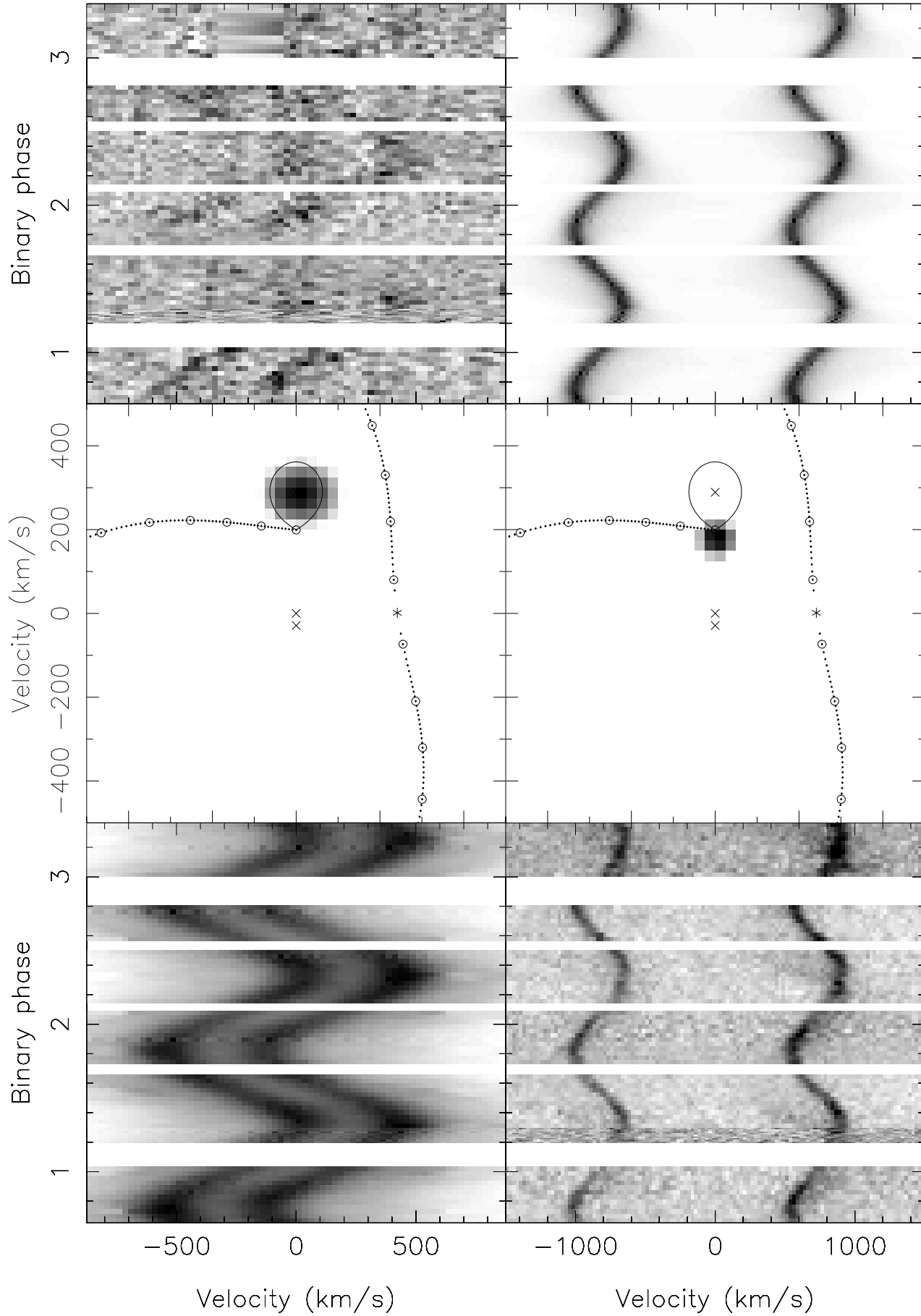




MR SER

Na I

Ca II



ST LMi

Na I

Ca II

